Water Research 266 (2024) 122362

Contents lists available at ScienceDirect

Water Research

journal homepage: www.elsevier.com/locate/watres

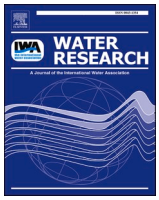

Drought reduces nitrogen supply and N_2O emission in coastal bays

Mingzhen Zhang [a,b], Dan Yu [b], Yiqi Yu [a,b], Ruifeng Yan [b], Yasong Li [c], Weijie Gong [d], Kai Xiao [e], Shaobin Li [b], Nengwang Chen [a,b,*]

[a] State Key Laboratory of Marine Environmental Science, Xiamen University, Xiamen, China
[b] Fujian Provincial Key Laboratory for Coastal Ecology and Environmental Studies, College of the Environment and Ecology, Xiamen University, Xiamen, China
[c] Institute of Hydrogeology and Environmental Geology, Chinese Academy of Geological Science, Shijiazhuang 050061, China
[d] College of Marine Science and Technology, Hainan Tropical Ocean University, Sanya 572022, China
[e] CAS Key Laboratory of Coastal Environmental Processes and Ecological Remediation, Yantai Institute of Coastal Zone Research, Chinese Academy of Sciences, Yantai 264003, China

ARTICLE INFO

Keywords:
Nitrogen cycling
Climate change
Greenhouse gas
Coastal bays
Groundwater discharge

ABSTRACT

Severe droughts are increasingly prevalent under global climate change, disrupting watershed hydrology and coastal nitrogen cycling. However, the specific effects of drought on nitrogen transport from land to sea and subsequent nitrogen dynamics remain inadequately understood. In this study, we evaluated the consequences of the 2020–2022 drought on nitrogen supply and N_2O emissions in Xiamen Bay, Southeast China. The results showed that drought significantly reduced annual NH_4—N, NO_2—N, and NO_3—N concentrations in Xiamen Bay by 49.4 %, 32.1 %, and 40.3 %, respectively, compared with the pre-drought year of 2019. The decline in NH_4—N concentration was mainly attributed to reduced surface runoff across all seasons. NO_3—N and NO_2—N concentrations declined only during spring and summer, primarily due to increased potential evapotranspiration (PET) hindering nitrogen supply via groundwater and concurrently enhancing land denitrification. Annual N_2O emission from Xiamen Bay decreased by 40.0~72.7 % during the drought, highly correlated with the decline in the concentrations of NO_3—N, DIN, and DTN ($p < 0.001$). Comparative analysis revealed that NO_3—N concentration exhibited consistent negative linear regressions with PET and declined as evaporative demand drought conditions worsened across Xiamen Bay, Sansha Bay, and Chesapeake Bay throughout 2010–2022. NH_4—N concentration showed a positive regression with river discharge in Xiamen Bay, but negative regressions in the other two bays. Our results indicates that drought reduces N_2O emission primarily driven by nitrate substrate reduction in the bay. This study provides new insights for predicting coastal nitrogen dynamics and greenhouse gas emissions under global environmental change.

1. Introduction

Climate change, combined with pervasive human activities, is accelerating the transition of El Niño Southern Oscillation (ENSO) phases (Cai et al., 2021), escalating the incidence and intensity of extreme weather events such as floods and droughts (Qu et al., 2020). These changes alter water cycle and its distribution on regional and global scales, affecting nutrient transport and transformation processes, and introducing huge uncertainty to aquatic ecosystems (Clark et al., 2015). Terrestrial nitrogen export to coastal waters has led to worldwide nitrogen over-enrichment, resulting in widespread coastal eutrophication, hypoxia, and acidification (Dai et al., 2023). This also influences global greenhouse gas emissions (e.g., N_2O, CH_4, CO_2) (Hutchins et al., 2022), particularly N_2O, which has a radiative forcing nearly 300 times that of CO_2 (Zhou et al., 2023). Currently, the responses of nitrogen and greenhouse gases in coastal waters to climate change are gaining increased attention. Compared with floods, relatively less attention has been paid to droughts, which however have increased frequency and severity in recent decades (Yuan et al., 2023).

Drought, characterized by anomalously low rainfall and heightened evapotranspiration (Zhao et al., 2022), significantly disrupts terrestrial hydrological connectivity, defined as the 'water-mediated transport of matter, energy, and organisms within and between elements of the hydrological cycle', and weakens the connectivity between land and sea (Castello et al., 2016; Pringle, 2001). During the drought summer of 2006, the riverine nitrate flux into the Changjiang Estuary was only 36.5

* Corresponding author at: College of the Environment and Ecology, Xiamen University, Xiamen 361102, PR China.
E-mail address: nwchen@xmu.edu.cn (N. Chen).

https://doi.org/10.1016/j.watres.2024.122362
Received 15 March 2024; Received in revised form 28 July 2024; Accepted 29 August 2024
Available online 10 September 2024

% of that observed during the flooding summer of 2020, with surface dissolved inorganic nitrogen (DIN) concentration reaching merely ~9 % of the latter (Sun et al., 2023). Despite an 86 % increase in groundwater-to-surface water transport during extreme drought compared to flood conditions, the reduced discharge during droughts extends water retention times, thereby facilitating nutrient transformation processes, as observed in the Lower Santa Fe River (Hensley et al., 2019). Drought-induced soil moisture depletion exacerbates water stress for evapotranspiration, effectively characterized by the Evaporative Demand Drought Index (EDDI) (Hobbins et al., 2016), which outperforms the traditional indices such as the Standardized Precipitation Index (SPI) and the Standardized Precipitation Evapotranspiration Index (SPEI) in predicting flash droughts over shorter timescales (Yao et al., 2018). While many studies have focused on material transport within river basins, few are designed for land-to-sea material transport (Dwivedi et al., 2018; Liu et al., 2019; Nevison et al., 2016), especially for groundwater transport, which is a critical yet often invisible component of the global hydrological cycle (Wang et al., 2023). Drought is an important factor influencing terrestrial hydrological conditions, yet its impact on the transport of terrestrial nitrogen to coastal seas remain unclear.

Coastal nitrogen primarily originates from river input, sewage effluents, groundwater discharges, and atmospheric deposition. Intensified human activities have significantly increased the contribution of sewage and agricultural runoff to coastal nitrogen levels in recent decades (Beusen et al., 2016; Li et al., 2023a; Luijendijk et al., 2020). Approximately 80 % of municipal wastewater is discharged untreated into coastal environments (Malone et al., 2020). Ammonia is usually the dominant nitrogen form in sewage effluent (Li et al., 2021). In semi-enclosed shallow bays such as Doha Bay, ammonia and nitrite levels exceed the Kuwait Environment Public Authority's maximum limits due to sewage discharge, accompanied by excessive levels of fecal coliform (Alkhalidi et al., 2022). Nitrate commonly holds high concentrations in groundwater owing to soil nitrification and subsequent leaching, with nitrogen leached from agricultural and nonagricultural sources contributing to widespread groundwater nitrate contamination (Gutiérrez et al., 2018). N_2O, a significant greenhouse gas, is predominantly produced through microbial nitrification and denitrification. Many factors, including microbial activity, temperature, electrical conductivity, and hydrologic conditions, influence N_2O production. Elevated N_2O concentrations are usually associated with high electrical conductivity, coinciding with higher nutrient levels and an abundance of N_2O-producing microbes across different land uses (Zhang et al., 2023). Field studies indicate that substrate nitrate concentration is a pivotal driver of N_2O emissions, overshadowing the impact of temperature (Yan et al., 2023b). Stream hydrology, particularly high-flow shifts, enhances nitrification, rather than denitrification in aquatic systems, as observed in the Wilson River in Australia, underscoring the control of hydrological factors on biogenic N_2O emissions (Wells et al., 2021). Nevertheless, the effects of drought on coastal N_2O emissions are insufficiently elucidated.

Here, we analyzed the drought effect on the highly urbanized Xiamen Bay in southeast China from 2020 to 2022, utilizing a comprehensive dataset encompassing meteorological and hydrological conditions, concentrations and isotopes of multiple nitrogen species, and other physicochemical parameters. The specific objectives of this study were to: (1) explore drought-induced changes in the concentrations of nitrogen species and N_2O levels in Xiamen Bay; (2) decipher how drought affects nitrogen dynamics in Xiamen Bay by altering land-to-sea transport processes; and (3) reveal the semi-quantitative relationships between drought characteristics and nitrogen concentrations in coastal bays.

2. Materials and methods

2.1. Study area

Xiamen Bay, a 390 km^2 marine expanse on the west coast of the Taiwan Strait, is segmented into four sea areas: Southern Xiamen Bay (SXB), Western Xiamen Bay (WXB), Tongan Bay (TAB), and Eastern Xiamen Bay (EXB) (Fig. 1a). The Jiulong River flows into SXB through the Jiulong River Estuary (JRE), with an annual freshwater discharge of 1.24×10^{10} m^3 (Chen et al., 2021). Xiamen bay is surrounded by the cities of Xiamen, Quanzhou, and Zhangzhou, with a combined population exceeding 5 million (Tab. S1). During the drought observation period, the socio-economic conditions around Xiamen Bay remained relatively stable. Built-up and agricultural lands adjacent to the bay accounted for about 33.4 % and 9.7 %, respectively (Fig. 1b). The upper Jiulong River basin is heavily agricultural, with excessive use of chemical fertilizers (Yu et al., 2015). As a semi-enclosed bay, Xiamen Bay has an average depth of ~10 m with almost no water stratification. The average residence time is approximately 16.5 days, and the tidal regime is predominantly semi-diurnal (Qian et al., 2023). Tidal systems in Xiamen Bay include the South China Sea Warm Current, branches of the Kuroshio Current and the Min-Zhe Coastal Currents (Cheng et al., 2021). The multi-year annual average temperature and precipitation are 21.6 °C and 1239.1 mm, respectively, with over 85 % of the annual precipitation occurring from March to August. Dissolved oxygen (DO) levels exhibited seasonal variability, with lower concentrations in spring and summer (234.4 ± 12.5 μmol L^{-1}) and higher values in winter and fall (278.1 ± 28.1 μmol L^{-1}). No significant annual changes were observed in water salinity, temperature, DO and pH throughout the observation period (Fig. S1, S2).

2.2. Sampling campaigns

A total of 12 sites were established around Xiamen Island (Fig. 1a). Between 2019 to 2022, fifteen seasonal sampling cruises were conducted onboard the "Ocean II", with winter (Win.), spring (Spr.), summer (Sum.), and fall (Fal.) samplings primarily occurring in January, April, July, and November, respectively. Seven cruises were selected to measure ammonia and nitrate isotopes (2019-Win., 2020-Sum., 2021-Spr., 2021-Sum., 2021-Fal., 2022-Win., and 2022-Fal.). Sediment samples were collected from four sites (X2, X7, X9, X12) in each sea area of Xiamen Bay during summer (July 2022) and winter (February 2023). Additionally, three sites (G1-G3) along the coast of WXB were designed for groundwater sampling. Physicochemical parameters were measured during spring (April 2022) and summer (July 2022), while nitrogen isotopes were analyzed in summer (July 2022), fall (November 2022), and winter (February 2023). Sampling for nitrogen isotopes of sewage endmembers in WXB and TAB was conducted in February 2019.

2.3. Sample collections and pretreatments

During seasonal cruises in Xiamen Bay, salinity, water temperature, DO, and pH were measured on board using a WTW multi-parameter portable meter (Multi 3630, Germany). Chlorophyll a (Chl a) was measured with an underway water ecological monitoring system (4H-JENA, Germany). Water samples were collected using 5 L Niskin bottle samplers, filtered through 0.7 μm pre-dried GF/F filters. Filtrates were divided into two portions: one was placed in pre-acid clean 50 mL centrifuge tubes, stored in cooling containers, and transported to the laboratory for analysis of dissolved nutrient concentrations within one week at 4 °C; the other portion was stored at −20 °C for subsequent nitrogen isotope measurements. Additional water samples for dissolved N_2O analysis were introduced into 60 mL brown glass bottles via a silicone tube directly from Niskin bottles, ensuring overflow of approximately three bottle volumes. To halt microbial activity, a final concentration of 0.1 % of saturated $HgCl_2$ was added and the bottles

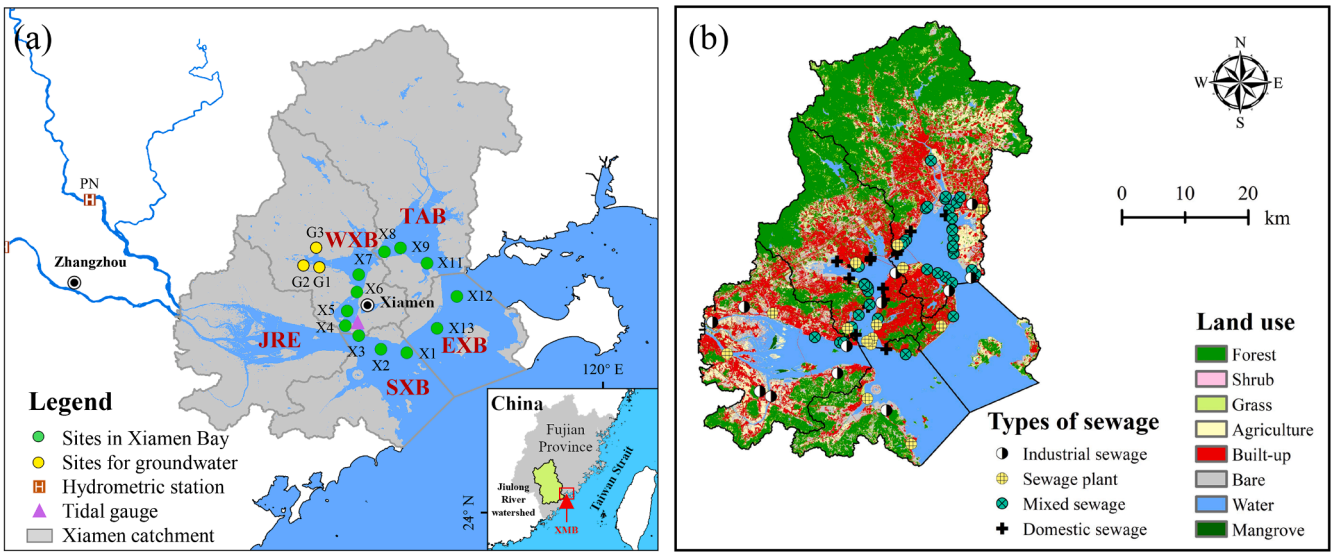

Fig. 1. Map of sampling sites (a), land use and distribution of sewage outlets (b) in the Xiamen Bay region (XMB). JRE, SXB, WXB, TAB, and EXB denote Jiulong River Estuary, Southern Xiamen Bay, Western Xiamen Bay, Tongan Bay, and Eastern Xiamen Bay, respectively.

were immediately sealed without air space.

Sediment samples were retrieved using a box corer, sealed in sterile ziplock bags, and preserved in chilled containers during transportation to the laboratory, where they were stored at −20 °C. Coastal groundwater samples were collected from porewater in sandy beaches and intertidal zones of WXB using a push-point piezometer. Salinity, conductivity, water temperature, and DO were measured with the same WTW multi-parameter portable meter (Multi 3630, Germany). Domestic sewage samples were obtained with a 5 L plexiglass container. Groundwater and sewage samples intended for nitrogen isotope analysis were treated identically to the seawater samples from Xiamen Bay.

2.4. Sample measurements

Dissolved nutrient concentrations were measured using an Auto-Analyzer 3 (Seal, Germany). Total dissolved nitrogen (DTN) was determined following digestion with 4 % alkaline potassium persulfate and analyzed as NO_3—N. Dissolved organic nitrogen (DON) was calculated as the difference between DTN and DIN (DIN = NH_4—N + NO_2—N + NO_3—N). Measurement precision for nutrients was assessed by repeating analysis on 10 % of the samples, with a relative error within 5 %. Isotopic ratios of $\delta^{15}N\text{-}NO_3^-$ and $\delta^{18}O\text{-}NO_3^-$ were determined using the denitrified method with an isotope ratio mass spectrometer 100 (IRMS, UK) (Sigman et al., 2001), while $\delta^{15}N\text{-}NH_4^+$ was measured via the diffusion method with an IRMS from Germany (Holmes et al., 1998). Dissolved N_2O concentration was analyzed with a gas chromatograph (Agilent 7890A, US) using the headspace equilibration technique. Detailed calculations for ΔN_2O (net N_2O concentration at the sea-air interface) and F_{N2O} (net N_2O flux at the sea-air interface) are outlined in Text S1. Sediment parameters, including moisture content, pH, Eh, total organic carbon (TOC), total nitrogen (TN), and nutrient contents are detailed in Text S3.

2.5. Auxiliary data collections

Land use was retrieved from the European Space Agency (https://viewer.esa-worldcover.org). Rainfall for Xiamen city and the Jiulong River watershed were sourced from the China Meteorological Data Network (http://data.cma.cn). Discharge for the main rivers flowing into Xiamen Bay and Sansha Bay were collected from local hydrological stations. Groundwater levels around Xiamen Bay were provided by the Institute of Hydrogeology and Environmental Geology, Chinese Academy of Geological Science. Global potential evapotranspiration (PET) was obtained from the Climatic Research Unit gridded Time Series (CRU TS v4.07) (https://crudata.uea.ac.uk). Discharge for rivers flowing into Chesapeake Bay were acquired from the Global Runoff Data Centre (https://portal.grdc.bafg.de). Long-term nutrient concentrations in Chesapeake Bay were obtained from the Chesapeake Bay Program data resources (https://datahub.chesapeakebay.net).

Terrestrial nitrogen inputs into Xiamen Bay were quantified by integrating five major sources: Jiulong River Estuary (JRE), sewage effluent (SW), atmospheric deposition (AD), small rivers (SR), and groundwater discharge (GW). Nitrogen inputs from JRE were calculated by multiplying river discharge by the estuarine effective nitrogen concentration, which was extrapolated from the conservative mixed line of nitrogen variation with salinity in the lower estuary. Nutrient sampling and measurement in JRE were conducted concurrently with those in Xiamen Bay. Nitrogen load from small rivers was yield by multiplying river discharge by nitrogen concentrations at river outlets, with small river discharge estimated based on Jiulong River discharge and the ratio between two catchment areas. Nitrogen concentrations for small rivers were obtained from the Xiamen City Environmental Monitoring Center Station. Annual riverine nitrogen load was computed by summing seasonal values. Annual sewage nitrogen load for 2021 was sourced from the Fujian Provincial Coastal Environmental Monitoring Center, with the assumption of stability throughout the study period given consistent socio-economic conditions. Atmospheric nitrogen deposition for 2016 was referenced from Wu et al. (2018) and assumed to be constant during the observation period. Groundwater nitrogen load was obtained by multiplying groundwater water mass by its nitrogen concentration, with annual groundwater discharge estimated using a water balance method as detailed in Text S4. Groundwater nitrogen concentration was cited from Hao et al. (2023).

2.6. Drought index calculations

Gamma distribution was applied to estimate the monthly Standard Runoff Index (SRI), where the cumulative probability of monthly runoff throughout the study period was obtained through maximum likelihood estimation (Shukla et al., 2008).

A non-parametric approach was employed to estimate EDDI, where empirically derived probabilities were obtained via an inverse normal approximation (Abramowitz et al., 1988). This probability-based method facilitated more consistent comparisons between EDDI against

other standardized indices (Won et al., 2020).

$$P(PET_i) = \frac{i - 0.33}{n + 0.33} \quad (1)$$

where $P(PET_i)$ is the empirical probability of PET_i, which is aggregated across the study period. i is the rank of aggregated PET in historical time series ($i = 1$ for the maximum PET). n denotes the number of observations in the series being ranked.

Then, SRI and EDDI were both derived from inverse normal approximation. Specifically, EDDI was calculated using the formula:

$$EDDI = W - \frac{C_0 + C_1 W + C_2 W^2}{1 + d_1 W + d_2 W^2 + d_3 W^3} \quad (2)$$

where the constants are defined as follows: $C_0 = 2.515517$, $C_1 = 0.802853$, $C_2 = 0.010328$, $d_1 = 1.432788$, $d_2 = 0.189269$, and $d_3 = 0.001308$. For $P \leq 0.5$, $W = (-2\ln P)^{1/2}$; For $P > 0.5$, replace P with [1-P] and reverse the sign of drought index.

2.7. Statistical analysis

One-way ANOVA was performed to test differences between sea areas following the Kolmogorov-Smirnov test and variance homogeneous test. The contributions of various nitrate sources were determined using the SIAR model, calculated in R 4.2.2 (as detailed in Text S2). Mantel analysis was chosen to explore the relationships between meteorological and hydrological parameters and physiochemical parameters

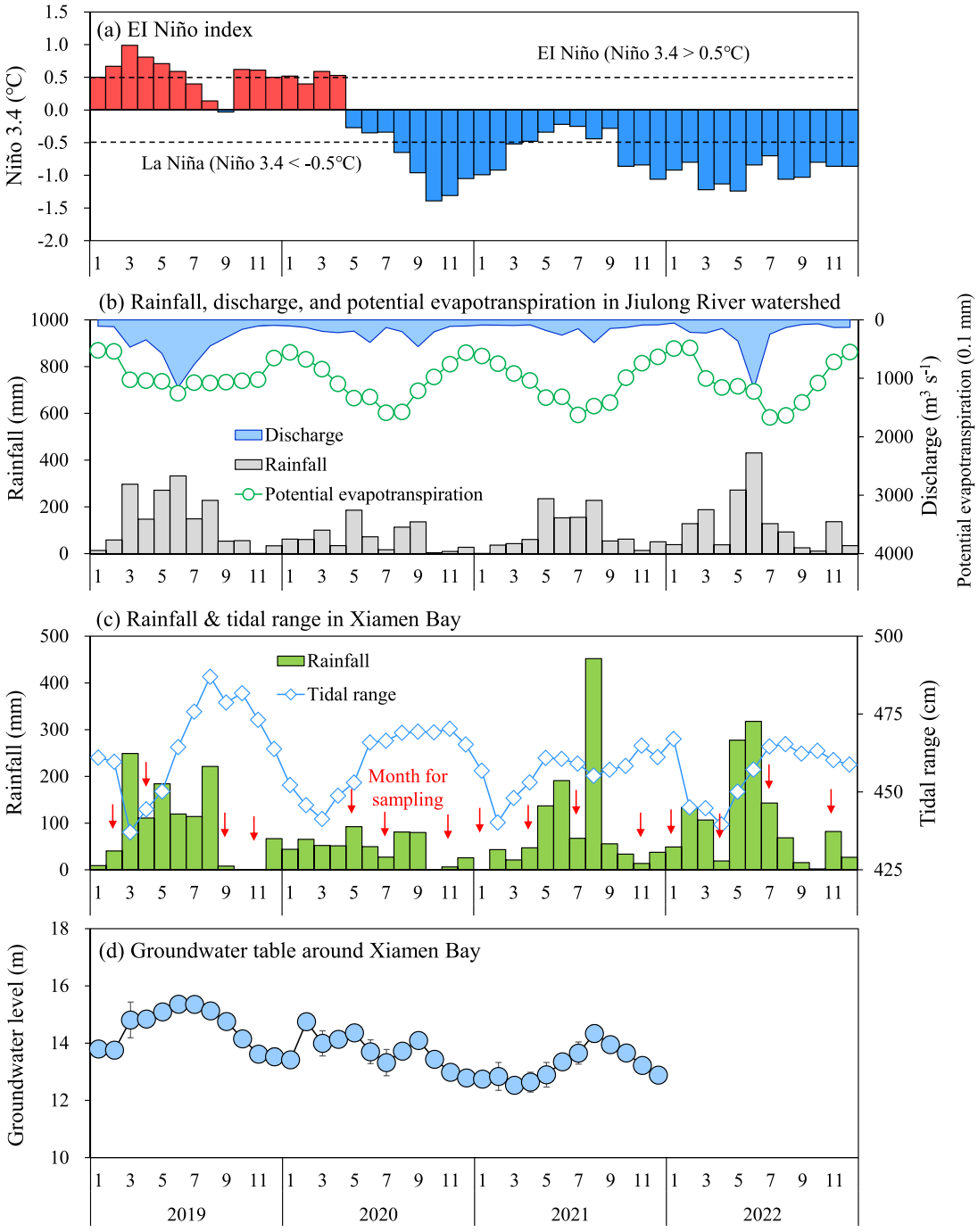

Fig. 2. Monthly variations of meteorological and hydrological conditions in the Xiamen Bay region (2019–2022). Groundwater level for 2022 is not available.

in Xiamen Bay. Linear regressions between parameters were implemented in Origin 2023 software, with significance levels indicated. All statistical tests were performed in SPSS 21.0. Data calculations and visualization were conducted using Origin 2023 and Python 3.11.

3. Results

3.1. Meteorological and hydrological conditions

The Niño 3.4 index remained positive throughout 2019, transitioning to negative from May 2020 until the end of 2022, indicative of the triple La Niña event during 2020–2022 (Fig. 2a). Annual rainfall in the Jiulong River watershed markedly decreased in 2020 (818.3 mm) compared to 2019 (1638.3 mm), but rebounded in 2021–2022 (1091.2 mm, 1520.7 mm) (Fig. 2b). Similar rainfall patterns were observed in Xiamen Bay (Fig. 2c), with reductions primarily occurring in spring and summer. Jiulong River discharge, however, was asynchronous with rainfall, registering 386.0, 203.2, 149.0, and 245.7 $m^3 s^{-1}$ from 2019 to 2022, reflecting a prolonged and delayed drought effect (Fig. 2b). Peak discharges in 2020 and 2021 decreased by 60.4 % and 66.4 % compared to 2019, with a time lag of 2~3 months. Annual PET increased in 2020–2022 (1040.1 mm, 1069.7 mm, 1044 mm) compared to 2019 (946.2 mm), with a ~20 % increase during spring and summer and minimal changes during fall and winter (Fig. 2b). The annual tidal range remained relatively constant throughout the study period, with higher values predominantly in the latter half of the year (Fig. 2c). Average groundwater levels around Xiamen Bay exhibited a slight decline from 2019 to 2021 (14.5 m, 13.8 m, 13.2 m) (Fig. 2d).

River discharge and PET were employed to characterize hydrological drought conditions and evaporative demand drought conditions, respectively (Fig. 3). SRI and EDDI were calculated to represent the specific timing and intensity of the drought. SRI exhibited no clear seasonal pattern, remaining almost entirely positive (indicating no hydrological drought) in 2019. In contrast, SRI turned negative (indicating hydrological drought) from May to September in 2020, remained negative for nearly the whole year in 2021 except for July and August, and was negative in January, April, and from August to October in 2022. EDDI generally was negative (indicating no evaporative demand drought) during fall and winter, and positive (indicating evaporative demand drought) during spring and summer. The average EDDI values during spring and summer in 2020–2022 (1.63 ± 0.53) were approximately double those of 2019 (0.83 ± 0.21), highlighting the increased evaporative demand drought during these periods.

3.2. Annual nitrogen loads from different external sources into Xiamen Bay

JRE and GW were the primary nitrogen sources during the study period, contributing on average 68.9 % and 23.5 % of the total DIN load, respectively (Fig. 4). SW was another significant source of NH_4—N, contributing an average of 15.9 %. The contributions of AD and SR to all nitrogen loads were less than 10 %. In the pre-drought year 2019, annual NH_4—N, NO_3—N, and DIN loads were 8300, 45,389, and 57,399 t yr^{-1}, respectively, with JRE being the largest nitrogen source, contributing 69 % of NH_4—N, 77 % of NO_3—N, and 77 % of DIN. All nitrogen loads significantly decreased in 2020, with annual NH_4—N, NO_3—N, and DIN loads reducing to 5206, 19,020 and 26,312 t yr^{-1}, respectively, although JRE remained the largest nitrogen source. There was a gradual increase in annual nitrogen load from 2020 to 2022. Nevertheless, both nitrogen load and contributions from JRE decreased from 2019 until 2021, while those from GW increased from their minimum in 2020 to their peak in 2021 and kept relatively stable in 2022. The maximum NH_4—N, NO_3—N, and DIN loads from GW was 1369, 11,278 and 12,693 t yr^{-1}, contributing an average of 21 %, 28 %, and 26 %.

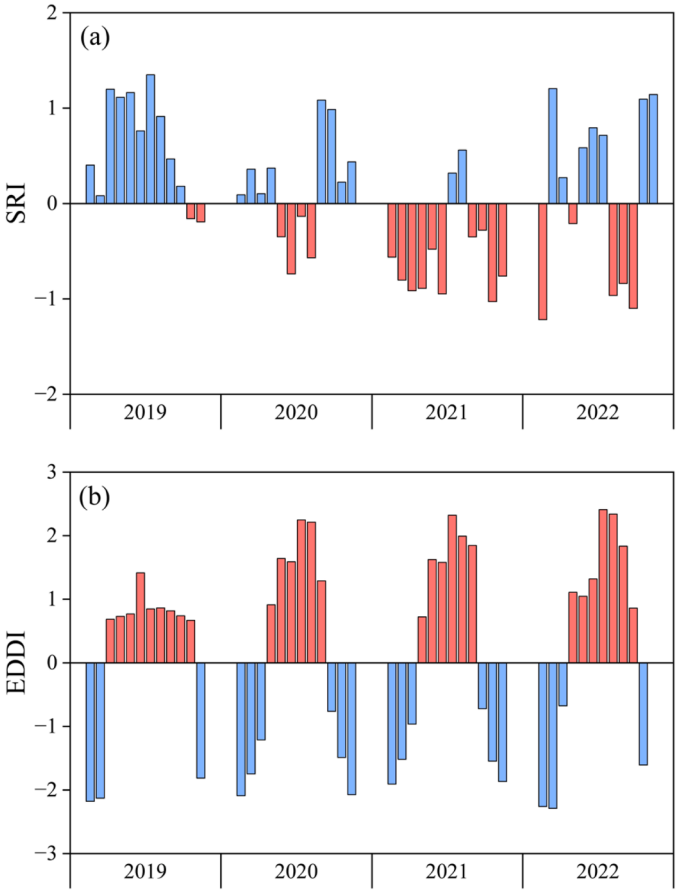

Fig. 3. Monthly variations of the Standardized Runoff Index (SRI) (a) and the Evaporative Demand Drought Index (EDDI) (b) in the Xiamen Bay region (2019–2022). Drought conditions are indicated by SRI values below −0.5 or EDDI values above 1, with drought severity increasing in line with the magnitude of the respective index.

3.3. Nitrogen species, N_2O, and nitrogen isotopes in Xiamen Bay

NO_3—N was the dominant nitrogen species in Xiamen Bay, accounting for 42.4~58.3 % of DTN (Fig. 5a-5d). The proportions of DON and NH_4—N in DTN were 24.0~29.5 % and 11.1~22.7 %, respectively. In 2019, NH_4—N and NO_2—N concentrations were higher during spring and summer than that in winter and fall. NO_3—N concentration peaked in winter and decreased until summer, then increased again after reaching a minimum in summer. Compared with 2019, annual concentrations of NH_4—N, NO_2—N, NO_3—N, and DON in 2020–2022 decreased on average by 49.4 %, 32.1 %, 40.3 %, and 16.6 %, respectively. Seasonally, NH_4—N concentration decreased across all seasons, while NO_2—N and NO_3—N mainly decreased substantially (77.3 %) during spring and summer and changed little during winter and fall. Spatially, nitrogen concentrations were higher in SXB, WXB, and TAB compared to EXB (Tab. S2), but the temporal variations among these four sea areas were generally consistent. Additionally, no significant differences in nitrogen concentrations were observed between surface and bottom water (Fig. S3a-S3d). The interannual and seasonal variations of ΔN_2O and F_{N2O} were consistent with NO_3—N (Fig. 5c, 5e, 5f), with ΔN_2O concentrations in the surface layer (22.1 ± 15.7 nmol L^{-1}) being about 10 % higher than those in the bottom layer (19.9 ± 15.0 nmol L^{-1}).

The nitrogen isotope results are shown in Fig. 6. In Xiamen Bay, $\delta^{15}N\text{-}NO_3^-$ steadily increased from winter 2019 (5.8 ± 2.0 ‰) to fall 2022 (19.9 ± 1.8 ‰). $\delta^{18}O\text{-}NO_3^-$ showed a similar trend, peaking at 14.5 ± 4.5 ‰ in spring 2021, and then stabilizing (7.1 ± 3.4 ‰). The $\Delta\delta^{15}N$-

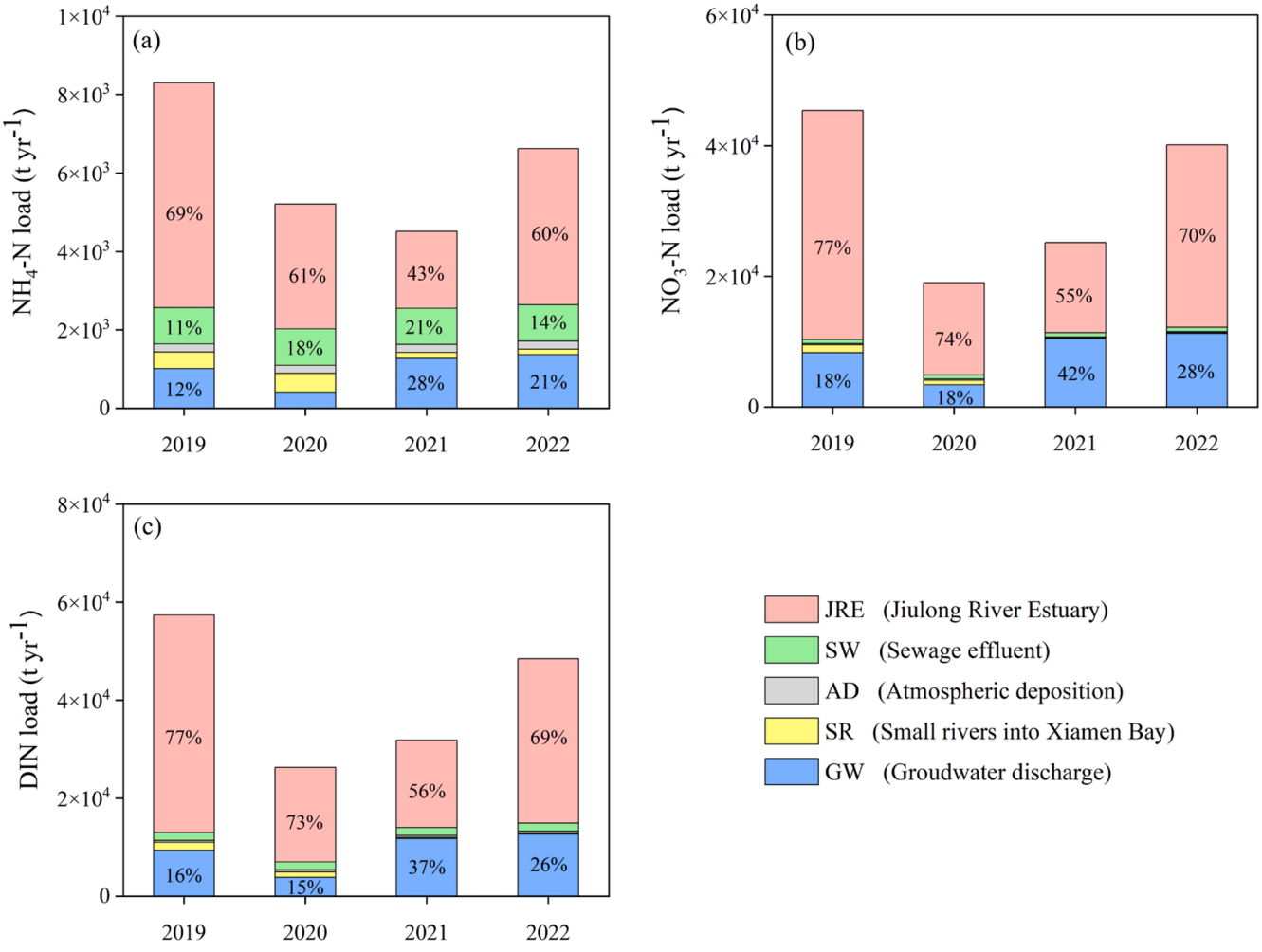

Fig. 4. Annual nitrogen inputs into Xiamen Bay from various external sources (2019–2022). Column values indicate the significant (>10 %) contributions to the annual nitrogen load. Riverine nitrogen loads were calculated by multiplying river discharge by measured nitrogen concentrations. Sewage nitrogen loads for 2021, sourced from the Fujian Provincial Coastal Environmental Monitoring Center, are assumed to be consistent throughout the study period, given the stable socio-economic conditions. Atmospheric nitrogen deposition data for 2016 are referenced from Wu et al. (2018). Groundwater discharge was estimated using the water balance principle described in Text S4, with corresponding nitrogen loads determined by applying the nitrogen concentrations reported by Hao et al. (2023).

NO_3^- : $\Delta\delta^{18}O\text{-}NO_3^-$ ratio during the study period ranged from 1.65 to 3.58. $\delta^{15}N\text{-}NH_4^+$ decreased during the drought observation. For end-members, groundwater $\delta^{15}N\text{-}NO_3^-$ and $\delta^{18}O\text{-}NO_3^-$ were 15.5 ± 8.4 ‰ and 11.7 ± 4.8 ‰, respectively, while sewage $\delta^{15}N\text{-}NO_3^-$, $\delta^{18}O\text{-}NO_3^-$, and $\delta^{15}N\text{-}NH_4^+$ were 16.6 ± 6.5 ‰, 1.0 ± 2.6 ‰, and 11.1 ± 3.2 ‰, respectively.

3.4. Sedimentary characteristics in Xiamen Bay

Sediments in Xiamen Bay were predominantly composed of silt, averaging 66.5 ± 5.8 ‰ (Tab. S3). Sediment pH and Eh values were 7.318 ± 0.142 and −17.7 ± 8.5 mV during summer, and 6.850 ± 0.155 and 10.3 ± 9.5 mV during winter (Tab. S4). The TN and TOC contents in sediments were 0.07 ± 0.01 % and 1.10 ± 0.06 % in summer, and 0.08 ± 0.04 % and 1.09±0.32 % in winter (Tab. S5). The C/N ratio averaged 15.6 ± 1.4 in summer and 15.9 ± 4.4 in winter. Contents of NH_4—N, NO_2—N, and NO_3—N were 137.2 ± 42.6, 0.23 ± 0.15, and 0.91 ± 0.17 μmol kg^{-1} in summer, and 106.1 ± 41.0, 0.49 ± 0.22, and 2.69 ± 1.00 μmol kg^{-1} in winter (Tab. S6). Ammonia was the dominant nitrogen species in the sediments accounting for approximately 98.1 %.

3.5. Relationships between physicochemical parameters with meteorological and hydrological conditions

A Mantel test was performed to show how meteorological and hydrological conditions affected physicochemical parameters in Xiamen Bay (Fig. 7). Salinity and pH displayed negative correlations with nitrogen species. Temperature was positively correlated with NH_4—N, but negatively correlated with NO_3—N, DIN, and DTN. The correlations between DO and nitrogen were the inverse of those between temperature and nitrogen. ΔN_2O showed a significant positive correlation with NO_3—N but no correlation with NH_4—N. Specifically, a per-unit increase in NO_3—N concentration (μmol L^{-1}) resulted in a 1.25-fold increase in ΔN_2O concentration (nmol L^{-1}) (Fig. S9b). Rainfall and tidal range did not significantly affect nitrogen species and ΔN_2O in Xiamen Bay ($p > 0.05$). The Niño 3.4 index and PET had significant impacts on NO_3—N, DIN, DTN, and ΔN_2O ($p < 0.05$). Discharge was the only factor with a significant impact on NH_4—N ($p < 0.05$).

4. Discussion

4.1. Major nitrogen sources in Xiamen Bay

In 2019, prior to the drought, the inconsistent seasonal timing in

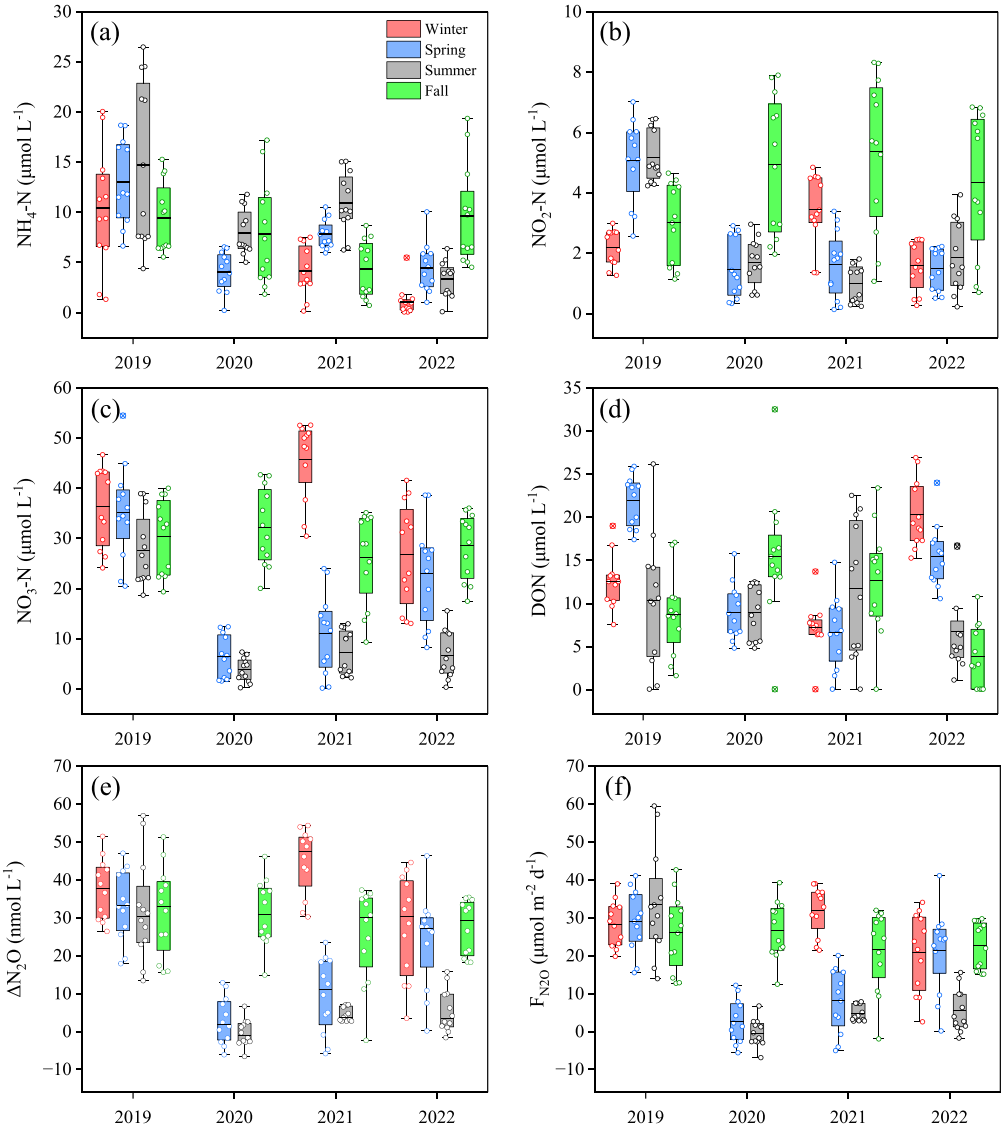

Fig. 5. Seasonal variations in nitrogen concentrations in surface seawater (a-d), ΔN_2O concentration (e) and N_2O flux (F_{N2O}, f) at the sea-air interface of Xiamen Bay (2019–2022). A positive ΔN_2O and F_{N2O} indicate net emission into the air, whereas negative values indicate net absorption by the sea. The central line represents the mean value, the box edges represent the interquartile range (IQR, 25th to 75th percentiles), the whiskers extend to the most extreme data points within 1.5 * IQR from the edges of the box, and the circles with × inside indicate outliers.

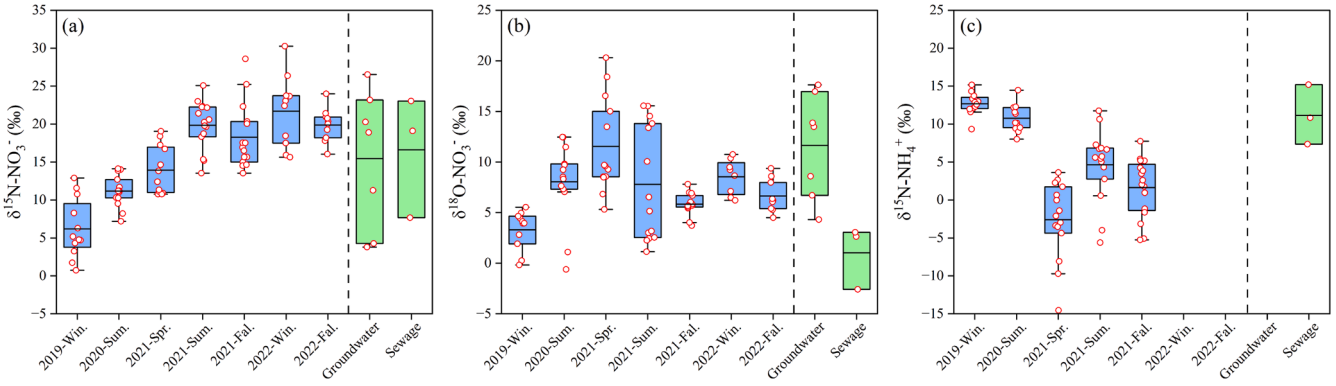

Fig. 6. Temporal variations of nitrogen isotopes in seawater of Xiamen Bay, alongside comparative isotope values from adjacent endmembers (groundwater, sewage) throughout the drought observation period. The central line represents the mean value, the box edges represent the interquartile range (IQR, 25th to 75th percentiles), the whiskers extend to the most extreme data points within 1.5 * IQR from the edges of the box.

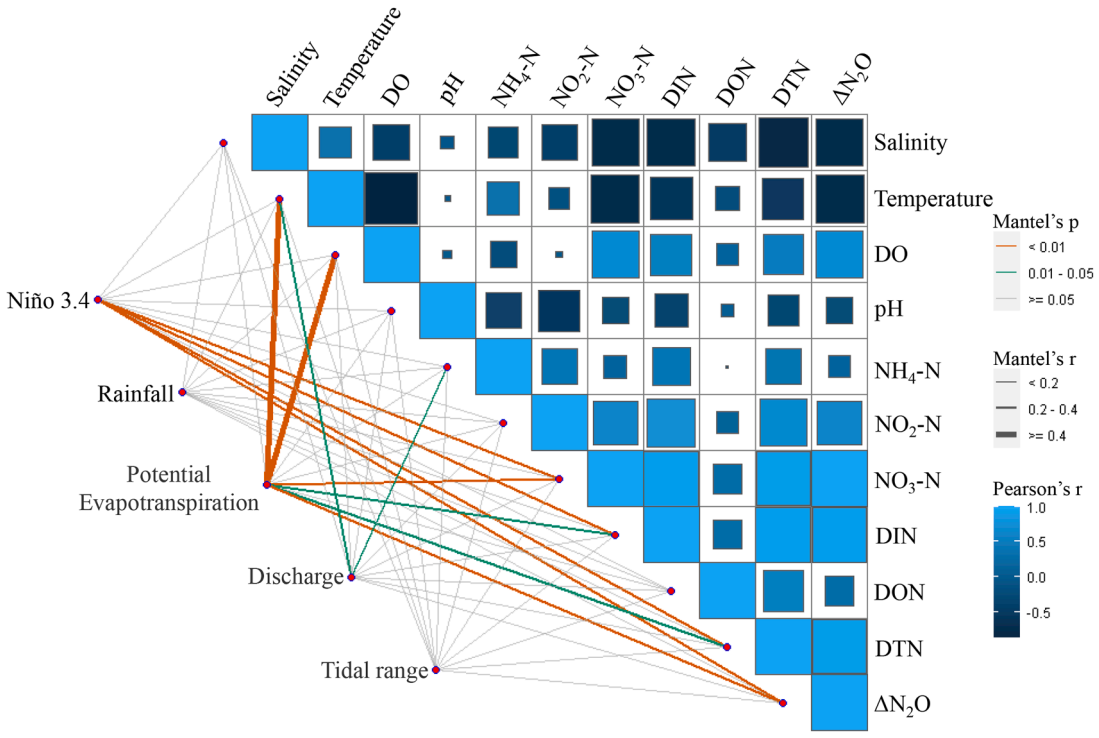

Fig. 7. Mantel test between physicochemical parameters with environmental conditions in Xiamen Bay. The mantel's p-value evaluates the statistical significance of relationships between two distance matrices, while the mantel's r-value quantifies the correlation strength. The pearson's r-value is employed to assess the liner correlations between paired variables.

nitrogen species suggested different terrestrial sources. Sewage was identified as the predominant NH_4—N source in Xiamen Bay, with the average $\delta^{15}N\text{-}NH_4^+$ during winter measured at 12.7 ‰ ± 0.4 ‰, aligning closely with the range of domestic sewage (11.1 ± 3.2 ‰) (Fig. 6c). NH_4—N from the Jiulong River is primarily derived from secondary sewage effluent and animal wastes (Lin et al., 2022). Despite JRE contributed the largest NH_4—N load overall (Fig. 4a), the highest concentrations were observed in TAB, followed by WXB and SXB (Tab. S2). This distribution is likely due to Jiulong River discharge mainly affecting SXB and the south area of WXB, with minimal impact on the north area of WXB and TAB (Cheng et al., 2021). The higher proportion of built-up land use in WXB (47.4 %) and TAB (39.4 %) compared to SXB (13.7 %) resulted in a significant local sewage contribution (Tab. S9). The elevated sewage NH_4—N load corresponded with higher NH_4—N concentration in the Bay (Fig. S7). NO_2—N exhibited a seasonal pattern akin to NH_4—N, likely due to shared sources, as nitrification produces nitrite as an intermediate (Fig. 5a, 5b). During spring and summer, increased surface runoff generated larger nitrogen fluxes, which may not be diluted upon entering Xiamen Bay, as revealed in studies on watershed (Gao et al., 2018) and coastal bays (Xu et al., 2010), causing higher NH_4—N and NO_2—N concentrations than in other seasons.

Fresh groundwater affected by agricultural activities is an important NO_3—N source in coastal bays (Wang et al., 2021). Nitrate in fresh groundwater primarily originates from the nitrification of N fertilizers applied to farmland (Hao et al., 2023), natural soil organic nitrogen (Wang et al., 2021), and surface ammonia pollutants (Han et al., 2023). In Xiamen Bay, groundwater NO_3—N concentrations range from 0.39 to 367.6 mg L^{-1}, with an average of 70.1 mg L^{-1}, largely due to agricultural activities (Hao et al., 2023). Results from the SIAR model, based on nitrate dual isotopes during winter 2019, indicated that ammonium fertilizer accounted for 66.7 % of nitrate sources in Xiamen Bay (Tab. S10), underscoring the substantial influence of terrestrial groundwater. Similarly, the Jiulong River's NO_3—N predominantly stems from excess ammonium fertilizer applied to upstream fields (Lin et al., 2022). NO_3—N concentrations were highest in WXB, followed by SXB and TAB (Tab. S2), with the combined effect of nitrate transport from Jiulong River discharge and local groundwater input likely contributing to the elevated nitrate concentrations in WXB compared to other sea areas. Winter is likely a period of great terrestrial fresh groundwater output, as sea level, driven by long-period solar tides, temperature, and winds, dominates over groundwater head as the largest contributor to the hydraulic gradient (Gonneea et al., 2013). Correspondingly, the highest NO_3—N concentration in Xiamen Bay was observed during winter (Fig. 5c). As seasons transitioned from winter to summer, NO_3—N concentration gradually decreased, likely due to the diminishing nitrate export from terrestrial fresh groundwater. Similarly, DIN fluxes from submarine groundwater discharge (SGD) were much higher during winter and fall than in spring and summer in both the Pearl River Estuary and the Changjiang River Estuary (Liu et al., 2018).

4.2. *Drought reduces terrestrial nitrogen input in Xiamen Bay*

Drought conditions curtailed surface runoff and diminished terrestrial ammonia load, consequently decreasing NH_4—N concentration and altering its seasonal and annual distributions within Xiamen Bay. Riverine NH_4—N loads from the Jiulong River Estuary and small rivers into Xiamen Bay substantially declined during the drought (Fig. 4). Compared to 2019, annual NH_4—N concentration decreased by 44.3 % in 2020, 42.8 % in 2021, and 61.0 % in 2022 (Fig. 5a). The unusual seasonal timing in 2020 showed unexpectedly low NH_4—N concentrations during spring and summer, reaching only 76.9 % of the fall within the same year, despite a decrease in fall NH_4—N concentration compared to the same period in 2019. This suggested that the impact of hydrological drought on the transport of surface materials may be particularly pronounced during spring and summer. Notably, both NH_4—N flux of Jiulong River and NH_4—N load from Jiulong River Estuary to Xiamen Bay during these seasons from 2020 to 2022 reduced by approximately 60 % relative to 2019, while remaining relatively consistent during winter and fall (Fig. S4-S5). These ammonia pollutants, which should have been flushed into the bay during wet seasons,

accumulated in the catchment due to the drought. This accumulation likely led to nitrification and subsequent leaching into deep groundwater during the following fall and winter (elaborated in next paragraph). In 2022, NH_4—N concentration was strikingly low from winter to summer, despite the recovery of riverine nitrogen load. Dynamic shifts in phytoplankton communities likely played a significant role in the observed reduction in NH_4—N concentration. Comparing with 2019, DON concentration elevated during the fall in 2020 and 2021, and the winter in 2022 (Fig. 5d). Correspondingly, there was also an increase in Chl a concentration during these periods compared with 2019 (Fig. S11). Interestingly, DON varied seasonally synchronously with Chl a ($p < 0.05$), yet inversely with NH_4—N in 2022 ($p < 0.01$). This may be due to changes in phytoplankton community structure, as Chl a concentration did not rise significantly. In July 2022, a marked transition in the phytoplankton community of Dongting Lake from diatoms to green algae and cyanobacteria was observed, coinciding with the most severe hydrometeorological drought since 1961 (Yan et al., 2023a). Chlorophyta is often accompanied by ammonia depletion, mainly driven by the simultaneous occurrence of cryptophyte blooms (María Concepción Lora, 2022). Phytoplankton blooms contribute to DON production in coastal waters, but the accumulation of DON contingents upon the type of phytoplankton bloom, particularly the species involved (Suksomjit et al., 2009). Consistently, DON fluxes from both the Jiulong River and its estuary significantly increased due to an approximately 4-fold increase in DON concentrations from winter to summer in 2022 (Fig. S4d, S5d). This suggests that the drought may also have caused notable changes in riverine phytoplankton community structures, warranting further comprehensive investigation. During the fall of 2022, cumulative rainfall five days preceding sampling was 125.2 mm in Jiulong River watershed and 11.3 mm in Xiamen Bay. Affected by this, NH_4—N concentration in Xiamen Bay approximated that observed in 2019, corresponding to a positive SRI value (no hydrological drought). Collectively, these findings underscore the role of hydrological drought, as indicated by river discharge, in modulating terrestrial nitrogen pollutant transport via surface runoff into the sea, and in governing the seasonal and interannual variability of NH_4—N concentration in Xiamen Bay. The potential impact of prolonged hydrological drought on phytoplankton community structure in nearshore continuum warrants serious consideration.

NO_3—N concentration exhibited distinct temporal changes from NH_4—N during the drought, probably due to different terrestrial sources and transport mechanisms. A negative regression ($p < 0.01$) between NO_3—N concentration and PET indicated a decrease in NO_3—N concentration in Xiamen Bay as surrounding PET increased (Fig. S8b). It has been shown that evapotranspiration frequently increases during droughts (Zhao et al., 2022). Compared to 2019, PET increased by ~5 % and ~30 % during spring and summer from 2020 to 2022, respectively (Fig. 2b). High evapotranspiration could deplete groundwater and damage shallow groundwater connectivity (Condon et al., 2020), resulting in lower soil moisture and weaker groundwater connections that produce longer hydraulic residence time and foster soil denitrification, especially during warmer seasons. In 2022, fresh groundwater DO (8.8 μmol L^{-1}) was lower than that saline groundwater (107.2 μmol L^{-1}) during summer (Tab. S7), potentially facilitating denitrification. In the adjacent Jiulong River Estuary, intense denitrification in the anoxic subterranean estuary led to high nitrate removal during summer (Hong et al., 2017). Denitrification rates in Xiamen Bay catchment were an order of magnitude higher during the drought summer of 2012 (Gao et al., 2013) than in the extremely wet year of 2016 (Zhang et al., 2018). Drought conditions, characterized by low soil moisture and elevated soil electrical conductivity, enhance denitrification potential and capacity (Li et al., 2018; Zhang et al., 2023). During severe droughts in managed grasslands, enhanced chemo- or co-denitrification dominates N_2O emissions due to reversible, drought-induced enrichment of nitrogen-bearing organic matter on soil microaggregates, despite well-oxygenated soils (Harris et al., 2021). Pérez et al. (2018) reported a 70 % increase in surface soil in-situ denitrification rates during rainless summers compared to wetter winters, with concurrent reductions in free-living diazotrophic activity and net N mineralization rates. It is hypothesized that the drought not only impeded nitrate transport towards the sea via subsurface pathways by disrupting groundwater connectivity but also reduced the nitrate pool through intensified denitrification, leading to a substantial decrease in NO_3—N concentration during spring and summer in Xiamen Bay (Fig. 5c). These processes likely altered the isotopic composition of transported nitrate, resulting in increased $\delta^{15}N\text{-}NO_3^-$ and $\delta^{18}O\text{-}NO_3^-$ in Xiamen Bay (Fig. 6a, 6b). During winter and fall, relatively normal PET and robust oceanic hydrodynamics facilitated greater groundwater nitrogen output, counteracting the NO_3—N concentration decrease from spring and summer and maintaining long-term stability. Notably, NO_3—N concentration was even higher in fall 2020 and winter 2021 compared to 2019, suggesting ammonium accumulated during drought was converted to nitrate through nitrification, replenishing the groundwater nitrate pool. Seasonal droughts reduce annual NO_3—N leaching, with non-spring droughts having legacy effects that increase NO_3—N leching in subsequent seasons (Liu et al., 2022). Correspondingly, the estimated NO_3—N load from GW was obvious high in 2021 (Fig. 4b). These processes may have altered terrestrial NO_2—N sources, which varied synchronously with NO_3—N following the drought onset. NO_2—N produced by nitrification from sewage effluents may have been consumed by enhanced denitrification and replenished by groundwater. Thus, the interaction of surface and groundwater, predominantly influenced by PET, likely regulates terrestrial nitrate transport to the coastal sea via groundwater, affecting NO_3—N concentration in Xiamen Bay. Further studies are necessary to elucidate the spatial-temporal distribution and regulatory mechanisms of groundwater nitrogen export to coastal sea.

4.3. Comparative analysis with other coastal systems globally

Linear regressions were employed to quantify significant changes in NH_4—N and NO_3—N concentrations in relation to river discharge and PET from 2019 to 2022 (Fig. S8). To verify these relationships, we integrated long-term monitoring data spanning 2010 to 2022 from three distinct coastal bays: Sansha Bay, an enclosed aquaculture bay in southeast China; Chesapeake Bay, the largest bay in the United States and a valley estuarine system; and Xiamen Bay. The comparative analysis revealed contrasting relationships between NH_4—N concentration and river discharge for Xiamen Bay versus Sansha Bay and Chesapeake Bay (Fig. 8a). Conversely, a consistent negative regression was observed between NO_3—N concentration and PET across all three bays (Fig. 8b). Concurrently, NH_4—N concentration did not exhibit discernible changes in response to the intensification of hydrological drought conditions (Fig. 8c), whereas NO_3—N concentration uniformly decreased as evaporative demand drought conditions worsened (Fig. 8d). This dichotomy suggests that ammonia is less sensitive to drought-induced hydrological alterations compared to nitrate. The uniform relationship between NO_3—N concentration and PET across the bays hints at a potential global prevalence of groundwater as an important source of nitrate in coastal bays, as per our previous analysis. Further data and evidence are required to confirm this hypothesis. Studies have indicated that nitrate inputs, driven by intensive anthropogenic activities and entering coastal waters through SGD, have escalated from 1.0 to 1.4 Tg per year over the second half of 20th century. This nitrate influx has become a significant contributor to the proliferation of harmful algal blooms (HABs) in coastal areas (Beusen et al., 2013; Lecher et al., 2015).

The observed negative regressions between NH_4—N concentration and discharge in Sansha Bay and Chesapeake Bay, in contrast to the positive regression in Xiamen Bay, were likely associated with the relatively modest river discharge in the former bays (Fig. 8a). During periods of reduced river discharge, such as those experienced during droughts, internal sources of ammonia, including benthic fluxes and reactions within porewaters, may become more pronounced. Murgulet

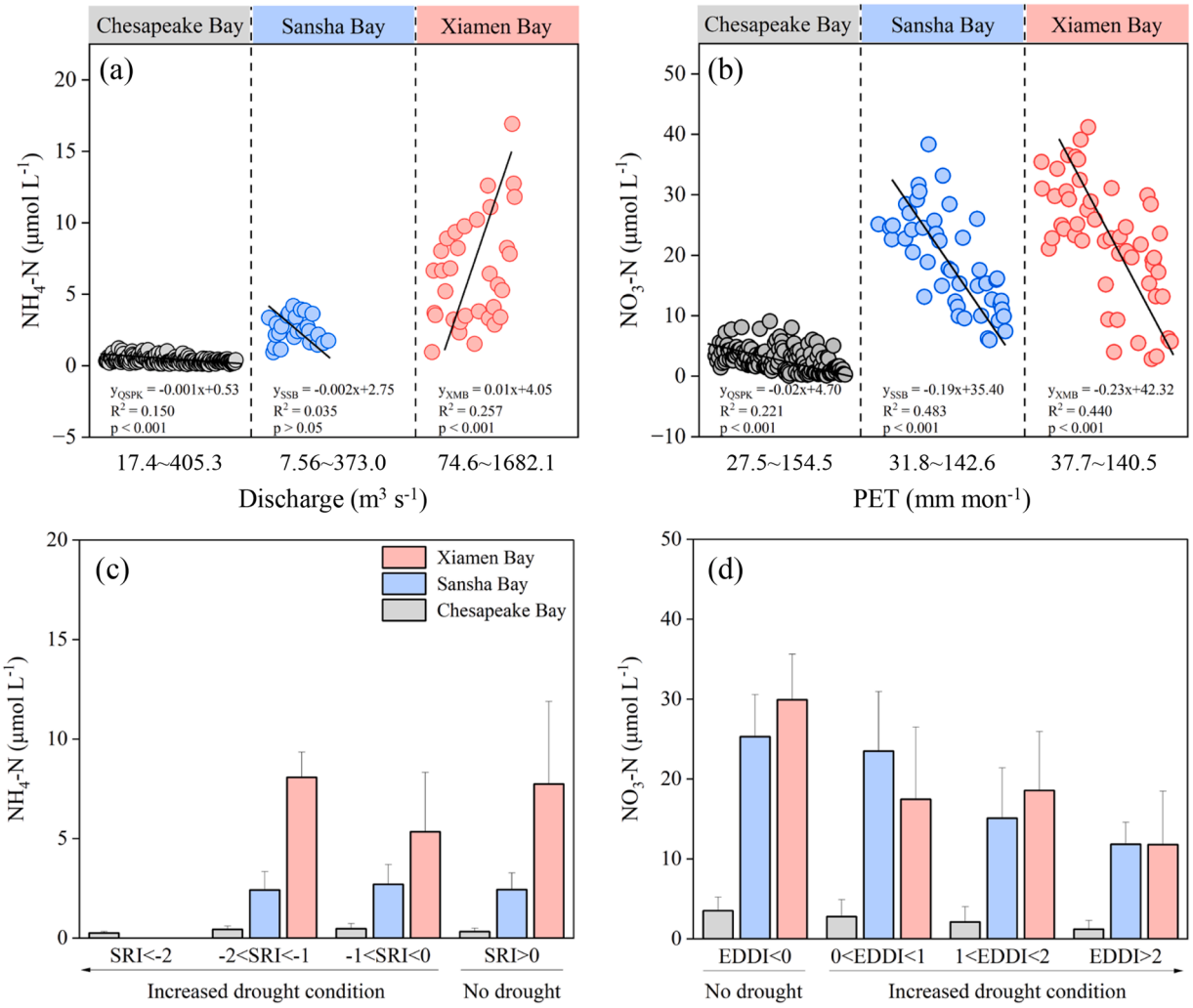

Fig. 8. Regression analysis of NH_4—N versus discharge (a) and NO_3—N versus potential evapotranspiration (PET) (b) in Xiamen Bay, Sansha Bay, and Chesapeake Bay (2010–2022). Normalized nitrogen concentrations in seawater under different drought conditions for NH_4—N (c) and NO_3—N (d). Nitrogen concentration was adjusted to a standard salinity of 35 for comparison.

et al. (2024) reported an increase in NH_4—N concentration during the hot and dry summer months, particularly within porewater, under increasingly reducing conditions in Baffin Bay. This increase was primarily attributed to sediment dissimilatory nitrate reduction to ammonia (DNRA), modulated by the degradation or mineralization of organic matter. In Xiamen Bay, sediment NH_4—N concentrations were also notably higher during the summer of 2022 (137.1 ± 42.9 μmol kg^{-1}) compared to the winter (106.4 ± 40.7 μmol kg^{-1}), contrary to the seasonal distribution of NO_3—N (Tab. S6). In contrast to the behavior of nitrate dual isotopes, $\delta^{15}N\text{-}NH_4^+$ decreased during the drought observation (Fig. 6c), suggesting a potential enhancement of mineralization or DNRA processes. The typical $\delta^{15}N\text{-}NH_4^+$ signature for ammonia derived from mineralization ranges from −7 ‰ to −1 ‰, significantly lower than that originating from domestic sewage (7 ‰~17 ‰) and manure (21 ‰ ~35 ‰) (Cao et al., 2022). The observed increase in DNRA may be mainly attributed to the increased proportion of autochthonous organic matter, resulting from reduced man-made pollution (Aalto et al., 2021). Nevertheless, despite these processes, the apparent NH_4—N concentration in Xiamen Bay still decreased during the drought, probably due to the minor contribution of sediment DNRA to the overall ammonia load. This observation indirectly underscores the pivotal role of terrestrial exogenous input in determining ammonia concentrations in the bay.

4.4. *Drought conditions regulate N_2O emission in Xiamen Bay*

The alleviation of drought-induced nitrogen pollution weakened N_2O emissions in Xiamen Bay (Fig. 5e, 5f), with the annual N_2O flux at the sea-air interface decreasing by 40.0~72.7 % compared to 2019, averaging a reduction of 52.0 %. This decline was primarily attributed to reduced concentrations of NO_3—N, DIN, and DTN (Fig. 7), indicating denitrification as a significant N_2O source in Xiamen Bay. Traditionally, nitrification has been considered the largest marine N_2O source (Frame et al., 2014). However, recent studies have highlighted that in oxic coastal waters and sediments, particle-associated denitrification (Wan et al., 2023) and chemo-denitrification (Li et al., 2023b) are the main sources of N_2O. Employing a global warming potential (GWP_{100}) calculated over a 100-year time scale, the reduction in GWP_{100} of N_2O during the drought in Xiamen Bay was estimated to be 5.0~9.1 × 10^8 mol yr^{-1}, equivalent to 67.6~350 % of the recorded CO_2 emission (2.6~7.4 × 10^8 mol yr^{-1}) (Dai et al., 2009). This suggested that the drought, triggered by the triple La Niña in 2020–2022, exerted negative feedback on global warming at a local scale by attenuating the nitrogen linkage between terrestrial and marine ecosystems.

The regression relationships (Fig. S8b, S9b) established in this study correlated PET and N_2O emissions, with NO_3—N concentration serving as a bridge, offering novel insights for predicting N_2O emissions under future climate change in analogous coastal bays, where nitrate was the

predominant nitrogen species. Drawing on the anticipated increase in PET trends within the humid and semi-humid regions of China, as gleaned from seven CMIP6 Shared Socioeconomic Pathway-Representative Concentration Pathway (SSP-RCP) scenarios (SSP119, SSP126, SSP434, SSP245, SSP460, SSP370, and SSP585) (Su et al., 2021), it was projected that NO_3—N concentrations in seawater of both Xiamen Bay and Sansha Bay would exhibit a declining trend from 2022 to 2100. For Xiamen Bay, specifically, an increment in PET per unit (mm mon^{-1}) was associated with an approximate reduction of 0.25 μmol L^{-1} in NO_3—N concentration. Consequently, the ΔN_2O concentration at the sea-air interface was projected to decrease from an average of 22.5 nmol L^{-1} during the current study period to 20.0 nmol L^{-1} in the timeframe of 2081–2100 (Table 1). Furthermore, the net N_2O flux emanating from Xiamen Bay was anticipated to decline from an average of 2.8×10^6 mol yr^{-1} to 2.6×10^6 mol yr^{-1}, considering the rise in future surface seawater temperature (SST) (Varela et al., 2023). Nonetheless, given the nonlinear response of N_2O production to nitrate removal, considerable uncertainty remains in forecasting N_2O emission in coastal bays (Yan et al., 2023b).

The protracted retention of land-based pollutants due to droughts will inevitably alter nitrogen cycling within terrestrial ecosystems and associated carbon cycles, thereby influencing the spatial distribution of greenhouse gas emission hotspots, and exerting either antagonistic or synergistic effects on the mitigation of nitrogen pollution in coastal bays (Ham et al., 2023; Qing et al., 2023). A meta-analysis demonstrates that drought conditions typically enhance the accumulation of soil DON, NH_4—N, and NO_3—N while concurrently reducing soil organic carbon and overall CO_2 emissions (Deng et al., 2021). Microbial activities in both temperate and tropical soil ecosystems are more susceptible to simulation under drought, leading to increased CO_2 and N_2O emissions, thus providing a robust positive feedback to global warming (Emmett et al., 2004). Additionally, with the increasing frequency of transitions between drought and flood events under climate change, accumulated bioavailable nitrogen is likely to be laterally transported offshore or vertically leached into deep groundwater during subsequent heavy precipitation events. This process could accelerate coastal eutrophication and foster the expansion of HABs (Paerl et al., 2018). It is imperative to conduct long-term studies on coastal water quality and greenhouse gas emissions throughout and after drought events to better understand and mitigate these complex environmental dynamics.

4.5. Uncertainties and limitations

The data used in this study predominantly comprised ground-based measurements and satellite remote sensing data (e.g., PET). The credibility of the findings can be influenced by the disparate origins of remote sensing databases. We performed a comparative analysis of the relationships between PET from various providers and nitrate concentrations across Xiamen Bay, Sansha Bay, and Chesapeake Bay for the period spanning 2010 to 2022. Our analysis revealed that the spatial resolution of remote sensing data significantly affected the quality of the derived PET. A notable discrepancy was observed between PET from the CRU TS v4.07 dataset with a 0.5° resolution and PET from the National Centers for Environmental Prediction-National Center for Atmospheric Research (NCEP-NCAR) Reanalysis 1 dataset with a 2.5° resolution (https://psl.noaa.gov/data/gridded/data.ncep.reanalysis.html) (Tab. S13). This discrepancy was particularly pronounced for smaller coastal bays such as Xiamen Bay and Sansha Bay, whereas it was less evident for the larger Chesapeake Bay (Tab. S14). To enhance the accuracy of our comparisons for Xiamen Bay and Sansha Bay, we incorporated an additional dataset, the National Tibetan Plateau / Third Pole Environment Data Center (TPDC) with a 1 km resolution (https://data.tpdc.ac.cn/zh-hans/data). Ultimately, the results indicated that the standard deviations in the relationships between PET derived from different sources and nitrate concentrations were less than 3 %.

This study acknowledges several potential limitations. Due to constraints in data collection and observation (e.g., groundwater discharge), the comparative analysis was restricted to four coastal bays. Our results indicated both negative and positive regressions between coastal NH_4—N concentration and river discharge, whereas a consistently negative regression was observed between coastal NO_3—N concentration and PET. Additionally, the predictive accuracy of coastal nitrate concentrations and N_2O emissions under varying climate change scenarios was contingent on the reliability of PET and SST. The effectiveness of PET and SST predictions inherently rely on the choice of appropriate climate models and how well they perform. Future research should pay more attention to drought effects on the transport of materials from diverse terrestrial sources to coastal bays, focusing on the response of terrestrial nitrogen or carbon cycling to different hydroclimatic conditions, and exploring the global universality of drought effects.

Table 1
Prediction results of NO_3—N, ΔN_2O, and F_{N2O} in Xiamen Bay based on PET evolution under CMIP6 SSP-RCP scenarios.

Parameter	Reference	2021–2040	2041–2060	2081–2100	Source
PET (mm mon^{-1})	78.4 (74.1, 82.0)	81.7 (77.4, 86.0)	83.8 (79.6, 88.2)	87.0 (82.9, 92.9)	(Su et al., 2021)
NO_3—N (μmol L^{-1})	23.1 (3.8, 45.6)	22.4 (3.0, 44.6)	21.9 (2.5, 44.1)	21.1 (1.8, 43.1)	This study
ΔN_2O (nmol L^{-1})	22.5 (−0.4, 44.8)	21.5 (−1.3, 43.6)	20.9 (−2.0, 43.0)	20.0 (−2.9, 41.7)	This study
F_{N2O} (10^5 mol yr^{-1})	28.0 (−0.5, 55.8)	27.0 (−1.7, 54.7)	26.6 (−2.5, 54.8)	26.4 (−3.8, 54.9)	This study

Note: The data format is average (minimum, maximum). PET denotes potential evapotranspiration. A positive ΔN_2O and F_{N2O} indicate net emission into the air, whereas negative values indicate net absorption by the sea.

5. Conclusions

The 2020–2022 drought had a marked impact on nitrogen concentrations and N_2O emissions in Xiamen Bay, Southeast China. Throughout this period, NH_4—N concentration experienced seasonal reductions year-round, while NO_2—N and NO_3—N concentrations declined only during spring and summer. A negative correlation between ΔN_2O and NO_3—N, DIN, and DTN, suggests a significant role of denitrification. The observed increases in $\delta^{15}N\text{-}NO_3^-$ and $\delta^{18}O\text{-}NO_3^-$, alongside a decrease in $\delta^{15}N\text{-}NH_4^+$, indicate changes in nitrogen sources and transformations driven by the drought. Despite the drought conditions, variations in rainfall and tidal range had minimal influence on nitrogen dynamics. In contrast, Niño 3.4 index and PET exhibited significant negative correlations with NO_3—N, DIN, DTN, and ΔN_2O, whereas NH_4—N was positively correlated only with river discharge, highlighting its distinct behavior relative to NO_3—N. The reduction in surface runoff due to the drought led to decreased terrestrial pollutant inputs, notably affecting NH_4—N concentration and its seasonal variations. Phytoplankton community changes, especially in 2022, likely contributed to the observed NH_4—N reductions. Increased PET during spring and summer was linked to declines in NO_3—N concentration, attributed to reduced groundwater nitrogen supply and enhanced land denitrification. In contrast to NH_4—N, NO_3—N concentration was proved to be more sensitive to drought-induced changes in hydrological processes, which exhibited consistent negative linear regressions with PET and decreased as evaporative demand drought conditions worsened across Xiamen Bay, Sansha Bay, and Chesapeake Bay throughout 2010–2022. NH_4—N concentration held positive regression with river discharge in Xiamen Bay, but negative regressions in the other two bays.

Our study implied that alterations in nitrogen source supply and greenhouse gas emissions in coastal bays, driven by droughts, constitute

one of the crucial feedback mechanisms for global climate change. This underscores the intricate interplay among hydrological conditions, biological processes, and nutrient dynamics within coastal ecosystems. A particular emphasis is placed on the role of PET in modulating nitrate availability and the potentially far-reaching impact of groundwater on nutrient concentrations in coastal bays. The observed correlations between terrestrial nitrogen inputs and the bay's nitrogen dynamics illustrate the profound influence of land-derived nitrogen pollution on the water quality and ecological health in these coastal environments. These insights underscore the critical need for an integrated land-sea management approach and the imperative to foster a resilient bay ecosystem.

CRediT authorship contribution statement

Mingzhen Zhang: Writing – review & editing, Writing – original draft, Visualization, Validation, Software, Methodology, Investigation, Formal analysis, Data curation, Conceptualization. **Dan Yu:** Writing – review & editing. **Yiqi Yu:** Software, Methodology, Investigation. **Ruifeng Yan:** Writing – review & editing, Investigation. **Yasong Li:** Investigation. **Weijie Gong:** Investigation. **Kai Xiao:** Writing – review & editing. **Shaobin Li:** Writing – review & editing. **Nengwang Chen:** Writing – review & editing, Supervision, Resources, Project administration, Funding acquisition.

Declaration of competing interest

We declare that (1) this manuscript contains original scientific research that has not been published elsewhere previously and (2) all authors listed on the above-referenced manuscript are aware of the submission to this journal.

Data availability

Data will be made available on request.

Acknowledgements

This study was supported by the Science and Technology Program of Xiamen, China (No. 3502Z20226021), the Science and Technology Program of Fujian Province, China (No. 2023Y4001), the National Natural Science Foundation of China (No. 41676098), and the PhD Fellowship of the State Key Laboratory of Marine Environmental Science at Xiamen University. We thank Yao Wang, Junou Du, Xuwen Fang, Shaowei Zheng, Qichen Hao and Yuewen Zhao for their assistants in field work and lab analysis.

Supplementary materials

Supplementary material associated with this article can be found, in the online version, at doi:10.1016/j.watres.2024.122362.

References

Aalto, S.L., Asmala, E., Jilbert, T., Hietanen, S., 2021. Autochthonous organic matter promotes DNRA and suppresses N_2O production in sediments of the coastal Baltic Sea. Estuar. Coast. Shelf Sci. 255.

Abramowitz, M., Stegun, I.A., Romer, R.H., 1988. Handbook of mathematical functions with formulas, graphs, and mathematical tables. Am. J. Phys. 56 (10), 958.

Alkhalidi, M.A., Al-Nasser, Z.H., Al-Sarawi, H.A., 2022. Environmental impact of sewage discharge on shallow embayment and mapping of microbial indicators. Front. Environ. Sci. 10, 1–12.

Beusen, A.H.W., Bouwman, A.F., Van Beek, L.P.H., Mogollón, J.M., Middelburg, J.J., 2016. Global riverine N and P transport to ocean increased during the 20th century despite increased retention along the aquatic continuum. Biogeosciences 13 (8), 2441–2451.

Beusen, A.H.W., Slomp, C.P., Bouwman, A.F., 2013. Global land–ocean linkage: direct inputs of nitrogen to coastal waters via submarine groundwater discharge. Environ. Res. Lett. 8 (3), 034035.

Cai, W.J., Santoso, A., Collins, M., Dewitte, B., Karamperidou, C., Kug, J.S., Lengaigne, M., McPhaden, M.J., Stuecker, M.F., Taschetto, A.S., Timmermann, A., Wu, L.X., Yeh, S.W., Wang, G.J., Ng, B., Jia, F., Yang, Y., Ying, J., Zheng, X.T., Bayr, T., Brown, J.R., Capotondi, A., Cobb, K.M., Gan, B.L., Geng, T., Ham, Y.G., Jin, F.F., Jo, H.S., Li, X.C., Lin, X.P., McGregor, S., Park, J.H., Stein, K., Yang, K., Zhang, L., Zhong, W.X., 2021. Changing El Niño–Southern Oscillation in a warming climate. Nat. Rev. Earth Env. 2 (9), 628–644.

Cao, M.D., Yin, X.J., Zhang, J., Jin, M.G., Huang, X., 2022. Sources and transformations of nitrogen in an agricultural watershed on the Jianghan Plain, China: an integration of $\delta^{15}N$–NH_4^+, $\delta^{15}N$–NO_3^-, $\delta^{18}O$–NO_3^- and a Bayesian isotope mixing model. Appl. Geochem. 142, 105329.

Castello, L., Macedo, M.N., 2016. Large-scale degradation of Amazonian freshwater ecosystems. Glob. Chang. Biol. 22 (3), 990–1007.

Chen, B.H., Wang, K., Dong, X., Lin, H., 2021. Long-term changes in red tide outbreaks in Xiamen Bay in China from 1986 to 2017. Estuar. Coast. Shelf Sci. 249, 107095.

Cheng, P., Wang, A.J., Wu, J.Z., Lin, Y.H., Chen, J.X., Chen, N.W., 2021. An assessment of residence and influence times in Xiamen Bay. China. Estuar. Coast. Shelf Sci. 262, 107595.

Clark, M.P., Fan, Y., Lawrence, D.M., Adam, J.C., Bolster, D., Gochis, D.J., Hooper, R.P., Kumar, M., Leung, L.R., Mackay, D.S., Maxwell, R.M., Shen, C.P., Swenson, S.C., Zeng, X.B., 2015. Improving the representation of hydrologic processes in Earth System Models. Water Resour. Res. 51 (8), 5929–5956.

Condon, L.E., Atchley, A.L., Maxwell, R.M., 2020. Evapotranspiration depletes groundwater under warming over the contiguous United States. Nat. Commun. 11 (1), 873.

Dai, M.H., Lu, Z.M., Zhai, W.D., Chen, B.S., Cao, Z.M., Zhou, K.B., Cai, W.J., Chenc, C.T. A., 2009. Diurnal variations of surface seawater pCO_2 in contrasting coastal environments. Limnol. Oceanogr. 54 (3), 735–745.

Dai, M.H., Zhao, Y.Y., Chai, F., Chen, M.R., Chen, N.W., Chen, Y.M., Cheng, D.Y., Gan, J. P., Guan, D.B., Hong, Y.Y., Huang, J.L., Lee, Y.T., Leung, K.M.Y., Lim, P.E., Lin, S.J., Lin, X., Liu, X., Liu, Z.Q., Luo, Y.W., Meng, F.F., Sangmanee, C., Shen, Y., Uthaipan, K., Wan Talaat, W.I.A., Wan, X.H.S., Wang, C., Wang, D.Z., Wang, G.Z., Wang, S.L., Wang, Y.M., Wang, Y.T., Wang, Z., Wang, Z.X., Xu, Y.P., Yang, J.Y.T., Yang, Y., Yasuhara, M., Yu, D., Yu, J.M., Yu, L.Q., Zhang, Z.K., Zhang, Z.L., 2023. Persistent eutrophication and hypoxia in the coastal ocean. Camb. prism., Coast. futures 1, e19.

Deng, L., Peng, C.H., Kim, D.G., Li, J.W., Liu, Y.L., Hai, X.Y., Liu, Q.Y., Huang, C.B., Shangguan, Z.P., Kuzyakov, Y., 2021. Drought effects on soil carbon and nitrogen dynamics in global natural ecosystems. Earth Sci. Rev. 214, 103501.

Dwivedi, D., Arora, B., Steefel, C.I., Dafflon, B., Versteeg, R., 2018. Hot spots and hot moments of nitrogen in a riparian corridor. Water Resour. Res. 54 (1), 205–222.

Emmett, B.A., Beier, C., Estiarte, M., Tietema, A., Kristensen, H.L., Williams, D., Peñuelas, J., Schmidt, I.K., Sowerby, A.J.E., 2004. The response of soil processes to cimate change: results from manipulation studies of shrublands across an environmental gradient. Ecosystems 7, 625–637.

Frame, C.H., Deal, E., Nevison, C.D., Casciotti, K.L., 2014. N_2O production in the eastern South Atlantic: analysis of N_2O stable isotopic and concentration data. Global Biogeochem. Cycles 28 (11), 1262–1278.

Gao, J.B., Wu, Q., Li, Q.L., Ma, J., Xu, Q.F., Groffman, P.M., Yu, S., 2013. Preliminary results from monitoring of stream nitrogen concentrations, denitrification, and nitrification potentials in an urbanizing watershed in Xiamen, southeast China. Int. J. Sust. Dev. World 20 (3), 223–230.

Gao, X.J., Chen, N.W., Yu, D., Wu, Y.Q., Huang, B.Q., 2018. Hydrological controls on nitrogen (ammonium versus nitrate) fluxes from river to coast in a subtropical region: observation and modeling. J. Environ. Manage. 213, 382–391.

Gonneea, M.E., Mulligan, A.E., Charette, M.A., 2013. Climate-driven sea level anomalies modulate coastal groundwater dynamics and discharge. Geophys. Res. Lett. 40 (11), 2701–2706.

Gutiérrez, M., Biagioni, R.N., Alarcón-Herrera, M.T., Rivas-Lucero, B.A., 2018. An overview of nitrate sources and operating processes in arid and semiarid aquifer systems. Sci. Total Environ. 624, 1513–1522.

Ham, Y.G., Kim, J.H., Min, S.K., Kim, D., Li, T., Timmermann, A., Stuecker, M.F., 2023. Anthropogenic fingerprints in daily precipitation revealed by deep learning. Nature 622 (7982), 301–307.

Han, L.L., Wang, H.L., Ge, L.H., Xu, M.N., Tang, J.M., Luo, L., Li, P., Kao, S.J., 2023. Transition of source/sink processes and fate of ammonium in groundwater along with redox gradients. Water Res. 231, 119600.

Hao, Q.C., Li, Y.S., Xiao, Y., Yang, H.J., Zhang, Y.Q., Wang, L.W., Liu, K., Liu, G.X., Wang, J., Hu, W.X., Liu, W.T., 2023. Hydrogeochemical fingerprint, driving forces and spatial availability of groundwater in a coastal plain, Southeast China. Urban Clim. 51, 101611.

Harris, E., Diaz-Pines, E., Stoll, E., Schloter, M., Schulz, S., Duffner, C., Li, K., Moore, K.L., Ingrisch, J., Reinthaler, D., Zechmeister-Boltenstern, S., Glatzel, S., Brüggemann, N., Bahn, M., 2021. Denitrifying pathways dominate nitrous oxide emissions from managed grassland during drought and rewetting. Sci. Adv. 7 (6), eabb7118.

Hensley, R.T., Kirk, L., Spangler, M., Gooseff, M.N., Cohen, M.J., 2019. Flow extremes as spatiotemporal control points on river solute fluxes and metabolism. J. Geophys. Res. Biogeosci. 124 (3), 537–555.

Hobbins, M.T., Wood, A., McEvoy, D.J., Huntington, J.L., Morton, C., Anderson, M., Hain, C., 2016. The evaporative demand drought index. Part I: linking drought evolution to variations in evaporative demand. J. Hydrometeorol. 17 (6), 1745–1761.

Holmes, R.M., McClelland, J.W., Sigman, D.M., Fry, B., Peterson, B.J., 1998. Measuring ^{15}N–NH_4^+ in marine, estuarine and fresh waters: an adaptation of the ammonia diffusion method for samples with low ammonium concentrations. Mar. Chem. 60 (3), 235–243.

Hong, Q.Q., Cai, P.H., Shi, X.M., Li, Q., Wang, G.Z., 2017. Solute transport into the Jiulong River estuary via pore water exchange and submarine groundwater discharge: new insights from $^{224}Ra/^{228}Th$ disequilibrium. Geochim. Cosmochim. AC. 198, 338–359.

Hutchins, D.A., Capone, D.G., 2022. The marine nitrogen cycle: new developments and global change. Nat. Rev. Microbiol. 20 (7), 401–414.

Lecher, A.L., Mackey, K., Kudela, R., Ryan, J., Fisher, A., Murray, J., Paytan, A., 2015. Nutrient loading through submarine groundwater discharge and phytoplankton growth in Monterey Bay, CA. Environ. Sci. Technol. 49 (11), 6665–6673.

Li, S.B., Cai, X.M., Niroula, S., Wallington, K., Gramig, B.M., Cusick, R.D., Singh, V., McIsaac, G., Oh, S., Kurambhatti, C., Emaminejad, S.A., John, S., 2023a. Integrated agricultural practices and engineering technologies enhance synergies of food-energy-water systems in corn belt watersheds. Environ. Sci. Technol. 57 (25), 9194–9203.

Li, S.B., Emaminejad, S.A., Aguiar, S., Furneaux, A., Cai, X.M., Cusick, R.D., 2021. Evaluating long-term treatment performance and cost of nutrient removal at water resource recovery facilities under stochastic influent characteristics using artificial neural networks as surrogates for plantwide modeling. ACS ES&T Eng. 1 (11), 1517–1529.

Li, X., Gao, D., Li, Y., Zheng, Y., Dong, H., Liang, X., Liu, M., Hou, L., 2023b. Increased nitrogen loading facilitates nitrous oxide production through fungal and chemodenitrification in estuarine and coastal sediments. Environ. Sci. Technol. 57 (6), 2660–2671.

Li, X., McCarty, G.W., Lang, M., Ducey, T., Hunt, P., Miller, J., 2018. Topographic and physicochemical controls on soil denitrification in prior converted croplands located on the Delmarva Peninsula, USA. Geoderma 309, 41–49.

Lin, J.J., Krom, M.D., Wang, F.F., Cheng, P., Yu, Q.B., Chen, N.W., 2022. Simultaneous observations revealed the non-steady state effects of a tropical storm on the export of particles and inorganic nitrogen through a river-estuary continuum. J. Hydrol. 606, 127438.

Liu, F., Zhu, Q., Zhou, Z.W., Liao, K.H., Lai, X.M., 2022. Soil nitrate leaching of tea plantation and its responses to seasonal drought and wetness scenarios. Agric. Water Manag. 260, 107325.

Liu, J.N., Du, J.Z., Wu, Y., Liu, S.M., 2018. Nutrient input through submarine groundwater discharge in two major Chinese estuaries: the Pearl River Estuary and the Changjiang River Estuary. Estuar. Coast. Shelf Sci. 203, 17–28.

Liu, S., Xie, Z.H., Zeng, Y.J., Liu, B., Li, R.C., Wang, Y., Wang, L.H., Qin, P.H., Jia, B.H., Xie, J.B., 2019. Effects of anthropogenic nitrogen discharge on dissolved inorganic nitrogen transport in global rivers. Glob. Chang. Biol. 25 (4), 1493–1513.

Luijendijk, E., Gleeson, T., Moosdorf, N., 2020. Fresh groundwater discharge insignificant for the world's oceans but important for coastal ecosystems. Nat. Commun. 11 (1), 1260.

Malone, T.C., Newton, A., 2020. The globalization of cultural eutrophication in the coastal ocean: causes and consequences. Front. Mar. Sci. 7, 670.

María Concepción Lora, V., 2022. Prog. Microalgae Res. Leila Queiroz, Z., Eduardo, J.-L. Mariany Costa, D. (eds), p. Ch. 3, IntechOpen, Rijeka.

Murgulet, D., Lopez, C.V., Douglas, A.R., Eissa, M., Das, K., 2024. Nitrogen and carbon cycling and relationships to radium behavior in porewater and surface water: insight from a dry year sampling in a hypersaline estuary. Mar. Chem. 258, 104351.

Nevison, C., Hess, P., Riddick, S., Ward, D., 2016. Denitrification, leaching, and river nitrogen export in the Community Earth System Model. J. Adv. Model. Earth Syst. 8 (1), 272–291.

Paerl, H.W., Otten, T.G., Kudela, R., 2018. Mitigating the expansion of harmful algal blooms across the freshwater-to-marine continuum. Environ. Sci. Technol. 52 (10), 5519–5529.

Pérez, C.A., Armesto, J.J., 2018. Coupling of microbial nitrogen transformations and climate in sclerophyll forest soils from the Mediterranean Region of central Chile. Sci. Total Environ. 625, 394–402.

Pringle, C., 2001. Hydrologic connectivity and the management of biological reserves: a global perspective. Ecol. Appl. 11, 981–998.

Qian, L.Y., Wang, F.F., Cao, W., Ding, S., Cao, W.Z., 2023. Ecological health assessment and sustainability prediction in coastal area: a case study in Xiamen Bay. China. Ecol. Indic. 148, 110047.

Qing, Y.M., Wang, S., Yang, Z.L., Gentine, P., 2023. Soil moisture−atmosphere feedbacks have triggered the shifts from drought to pluvial conditions since 1980. Commun. Earth Environ. 4 (1), 254.

Qu, L.Y., Wu, Y.F., Li, Y., Stubbins, A., Dahlgren, R.A., Chen, N.W., Guo, W.D., 2020. El Niño-driven dry season flushing enhances dissolved organic matter export from a subtropical watershed. Geophys. Res. Lett. 47 (19), e2020GL089877.

Shukla, S., Wood, A.W., 2008. Use of a standardized runoff index for characterizing hydrologic drought. Geophys. Res. Lett. 35 (2), L02405.

Sigman, D.M., Casciotti, K.L., Andreani, M., Barford, C., Galanter, M., Böhlke, J.K., 2001. A bacterial method for the nitrogen isotopic analysis of nitrate in seawater and freshwater. Anal. Chem. 73 (17), 4145–4153.

Su, B.D., Huang, J.L., Mondal, S.K., Zhai, J.Q., Wang, Y.J., Wen, S.S., Gao, M.N., Lv, Y.R., Jiang, S., Jiang, T., Li, A.W., 2021. Insight from CMIP6 SSP-RCP scenarios for future drought characteristics in China. Atmos. Res. 250, 105375.

Suksomjit, M., Nagao, S., Ichimi, K., Yamada, T., Tada, K., 2009. Variation of dissolved organic matter and fluorescence characteristics before, during and after phytoplankton bloom. J. Oceanogr. 65 (6), 835–846.

Sun, Q.W., Li, D.W., Wang, B., Xu, Z.S., Miao, Y.Y., Lin, H., Jin, H.Y., Jiang, Z.B., Zeng, J. N., Zhou, F., Chen, J.F., 2023. Massive nutrients offshore transport off the Changjiang Estuary in flooding summer of 2020. Front. Mar. Sci. 10, 1076336.

Varela, R., de Castro, M., Dias, J.M., Gómez-Gesteira, M., 2023. Coastal warming under climate change: global, faster and heterogeneous. Sci. Total Environ. 886, 164029.

Wan, X.S., Sheng, H.X., Liu, L., Shen, H., Tang, W.Y., Zou, W.B., Xu, M.N., Zheng, Z.Z., Tan, E., Chen, M.M., Zhang, Y., Ward, B.B., Kao, S.J., 2023. Particle-associated denitrification is the primary source of N_2O in oxic coastal waters. Nat. Commun. 14 (1), 8280.

Wang, X.J., Zhang, Y., Luo, M.H., Xiao, K., Wang, Q.Q., Tian, Y., Qiu, W.H., Xiong, Y., Zheng, C.M., Li, H.L., 2021. Radium and nitrogen isotopes tracing fluxes and sources of submarine groundwater discharge driven nitrate in an urbanized coastal area. Sci. Total Environ. 763, 144616.

Wang, Y.X., Yuan, S.H., Shi, J.B., Ma, T., Xie, X.J., Deng, Y.M., Du, Y., Gan, Y.Q., Guo, Z. L., Dong, Y.R., Zheng, C.M., Jiang, G.B., 2023. Groundwater quality and health: making the invisible visible. Environ. Sci. Technol. 57 (13), 5125–5136.

Wells, N.S., Eyre, B., 2021. Flow regulates biological NO_3^- and N_2O production in a turbid sub-tropical stream. Geochim. Cosmochim. Acta 306, 124–142.

Won, J., Choi, J., Lee, O., Kim, S., 2020. Copula-based Joint Drought Index using SPI and EDDI and its application to climate change. Sci. Total Environ. 744, 140701.

Wu, S.P., Dai, L.H., Wei, Y., Zhu, H., Zhang, Y.J., Schwab, J.J., Yuan, C.S., 2018. Atmospheric ammonia measurements along the coastal lines of Southeastern China: implications for inorganic nitrogen deposition to coastal waters. Atmos. Environ. 177, 1–11.

Xu, J., Yin, K.D., Lee, J.H.W., Liu, H., Ho, A.Y.T., Yuan, X.C., Harrison, P.J., 2010. Long-term and seasonal changes in nutrients, phytoplankton biomass, and dissolved oxygen in deep bay, Hong Kong. Estuaries Coast. 33 (2), 399–416.

Yan, G.H., Yin, X.Y., Wang, X., Zhang, Y.Y., Wang, E.R., Yu, Z.B., Ma, X.L., Huang, M.S., 2023a. Effects of summer and autumn drought on eutrophication and the phytoplankton community in Dongting lake in 2022. Toxics 11 (10), 822.

Yan, R.F., Wang, F.F., Wang, Y., Chen, N.W., 2023b. Pollution abatement reducing the river N_2O emissions although it is partially offset by a warming climate: insights from an urbanized watershed study. Water Res. 236, 119934.

Yao, N., Li, Y., Lei, T.J., Peng, L.L., 2018. Drought evolution, severity and trends in mainland China over 1961–2013. Sci. Total Environ. 616-617, 73–89.

Yu, D., Yan, W.J., Chen, N.W., Peng, B.R., Hong, H.S., Zhuo, G.H., 2015. Modeling increased riverine nitrogen export: source tracking and integrated watershed-coast management. Mar. Pollut. Bull. 101 (2), 642–652.

Yuan, X., Wang, Y.M., Ji, P., Wu, P.L., Sheffield, J., Otkin, J.A., 2023. A global transition to flash droughts under climate change. Sci 380 (6641), 187–191.

Zhang, S.B., Xia, X.H., Xin, Y., Li, X.K., Wang, J.F., Yu, L.L., Li, C.B., McDowell, W.H., Tan, Q., Yang, Z.F., 2023. Electrical conductivity as a reliable indicator for assessing land use effects on stream N_2O concentration. J. Hydrol. 626, 130253.

Zhang, Y., Ji, G.G., 2018. Quantitative responses of potential nitrification and denitrification rates to the size of microbial communities in rice paddy soils. Chemosphere 211, 970–977.

Zhao, M., A, G., Liu, Y.L., Konings, A.G., 2022. Evapotranspiration frequently increases during droughts. Nat. Clim. Chang. 12 (11), 1024–1030.

Zhou, J., Zheng, Y.L., Hou, L.J., An, Z.R., Chen, F.Y., Liu, B.L., Wu, L., Qi, L., Dong, H.P., Han, P., Yin, G.Y., Liang, X., Yang, Y., Li, X.F., Gao, D.Z., Li, Y., Liu, Z.F., Bellerby, R., Liu, M., 2023. Effects of acidification on nitrification and associated nitrous oxide emission in estuarine and coastal waters. Nat. Commun. 14 (1), 1380.